

# Hebbian STDP in mushroom bodies facilitates the synchronous flow of olfactory information in locusts

Stijn Cassenaer<sup>1</sup> & Gilles Laurent<sup>1</sup>

Odour representations in insects undergo progressive transformations and decorrelation<sup>1–3</sup> from the receptor array to the presumed site of odour learning, the mushroom body<sup>4–7</sup>. There, odours are represented by sparse assemblies of Kenyon cells in a large population<sup>2</sup>. Using intracellular recordings *in vivo*, we examined transmission and plasticity at the synapse made by Kenyon cells onto downstream targets in locusts. We find that these individual synapses are excitatory and undergo hebbian spike-timing dependent plasticity (STDP)<sup>8–10</sup> on a  $\pm 25$  ms timescale. When placed in the context of odour-evoked Kenyon cell activity (a 20-Hz oscillatory population discharge), this form of STDP enhances the synchronization of the Kenyon cells' targets and thus helps preserve the propagation of the odour-specific codes through the olfactory system.

Olfactory processing in insects begins in an array of receptor neurons that express collectively many tens of olfactory receptor genes ( $\sim 60$  in *Drosophila*<sup>11,12</sup>;  $\sim 150$  in honeybees<sup>13</sup>). The representations of general odours are then decorrelated by local circuits of projection neurons and local neurons in the antennal lobe<sup>1–3</sup>. In locusts and other insects, the antennal lobe output is distributed in space and time and can be described as stimulus-specific time-series of projection-neuron activity vectors, updated at each cycle of a 20-Hz collective oscillation<sup>1,14,15</sup>. Distributed projection-neuron activity is then projected to Kenyon cells, the intrinsic neurons of the mushroom body. In contrast to projection neurons, Kenyon cells respond very specifically and fire extremely rarely<sup>2</sup>. The mechanisms underlying this sparsening are starting to be understood<sup>2,16</sup>. Such sparse representations are advantageous for memory and recall<sup>16</sup>, consistent with established roles of the mushroom bodies in learning<sup>4–7</sup>. In *Drosophila*, experiments combining molecular inactivation with behaviour indicate that synaptic output from Kenyon cells in the lobes is required for memory retrieval<sup>5</sup>. Little is known, however, about the electrophysiological properties of these synapses.

We studied the connections made by Kenyon cells onto a small population of extrinsic neurons<sup>17</sup> in the  $\beta$ -lobe of the locust mushroom body (Fig. 1a), using an intact, *in vivo* preparation (Methods).  $\beta$ -lobe neurons ( $\beta$ -LNs) respond to odours; their responses are odour-specific and their tuning is sensitive to input synchrony<sup>17</sup>. We recorded intracellularly from pairs of Kenyon cells and  $\beta$ -LNs: randomly selected Kenyon cells were impaled in their soma;  $\beta$ -LNs were impaled in a dendrite in the  $\beta$ -lobe. We focused on one  $\beta$ -LN anatomical subtype<sup>17</sup>, which comprises many individual neurons. Neurons of this subtype, called  $\beta$ -LNs here, could be recognized also by their physiological characteristics (see below). Each  $\beta$ -LN has extensive dendrites (Fig. 1a, and Supplementary Fig. 1) that intersect many of 50,000 Kenyon cell axons. Monosynaptic connections were found in  $\sim 2\%$  of tested Kenyon cell (KC)– $\beta$ -LN pairs (Fig. 1b). All were excitatory. The delay between Kenyon cell spike and  $\beta$ -LN-excitatory post-synaptic potential (EPSP) onset was  $6.5 \pm 0.70$  ms,

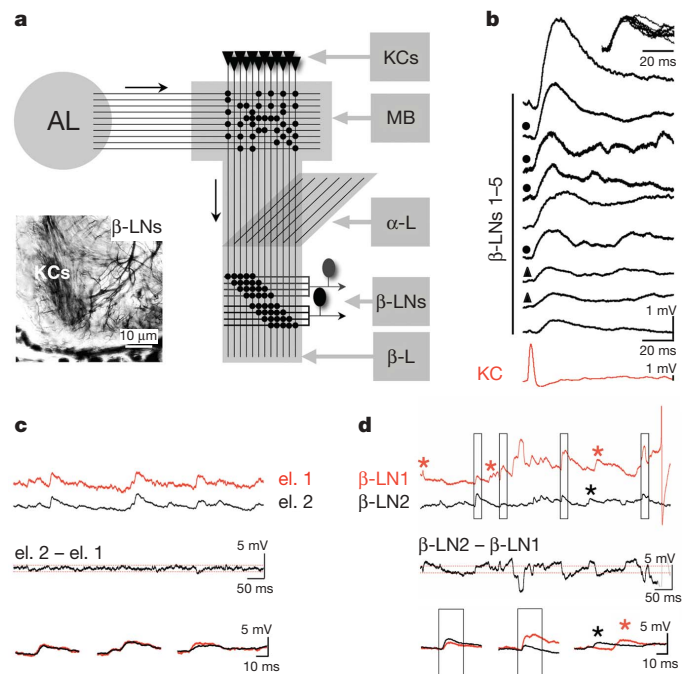


**Figure 1 | Synaptic connections between individual Kenyon cells and  $\beta$ -LNs are excitatory, powerful and varied in gain.** **a**, Schematic of the locust olfactory circuits: Projection neuron axons ( $n = 830$ ) exit the antennal lobe (AL) and send collaterals into the mushroom body (MB) calyx. There, they excite Kenyon cells ( $n = 50,000$ ) with  $\sim 50\%$  average connectivity<sup>16</sup>. Kenyon cells each send a bifurcating axon into the  $\alpha$ - and  $\beta$ -lobes ( $\alpha$ -L,  $\beta$ -L), forming ‘beams’ of thousands of tightly packed axons (inset). The finer dendrites of  $\beta$ -LNs run normal to Kenyon cell axons in  $\beta$ -LN-specific sectors: two of these can be seen in the inset (a photomicrograph of a 10- $\mu$ m-thick section of the distal end of the  $\beta$ -lobe). **b**, Spike-triggered averages of  $\beta$ -LN intra-dendritic recordings from nine different KC– $\beta$ -LN pairs (9 Kenyon cells, 5  $\beta$ -LNs). All  $\beta$ -LNs and Kenyon cells are recorded *in vivo*, with intracellular electrodes. Note the wide-range of spike-triggered average amplitudes. Same-symbol-marked spike-triggered averages are from the same  $\beta$ -LNs, with different presynaptic Kenyon cells sampled successively. Inset, scaled spike-triggered averages in **b**, illustrating similarity of kinetics. **c**, Simultaneous dendritic impalements of one  $\beta$ -LN with two separate electrodes (el. 1, 2). el. 2 – el. 1 is the difference between the two voltage traces; note the high correlation of amplitudes (noise envelope is 2 s.d., red stipples), indicating similar electrotonic access to synaptic sites. Lower panel, overlay of selected EPSPs from above. **d**, Simultaneous dendritic impalements of two different  $\beta$ -LNs (1 and 2). Note some common EPSPs (boxes) and EPSPs specific to either  $\beta$ -LN (\*).  $\beta$ -LN2 –  $\beta$ -LN1 is the difference between the two voltage traces; note significant variations on each side of the noise envelope (stippled lines as in panel **c**). Lower panel, overlay of selected EPSPs from above.

<sup>1</sup>California Institute of Technology, Division of Biology, 139-74, Pasadena, California 91125, USA.

including  $5.4 \pm 0.25$  ms for spike propagation from Kenyon cell soma to the  $\beta$ -lobe. The remaining (synaptic) delay ( $\sim 1$  ms) is similar to that at another chemical synapse in the locust brain<sup>16</sup>. Unitary EPSPs were large ( $1.58$  mV  $\pm$  1.11,  $n = 9$  pairs), in contrast to those generated in Kenyon cells by individual projection neurons ( $86$   $\mu$ V  $\pm$  44)<sup>16</sup>. The fact that Kenyon cell outputs are powerful is consistent with Kenyon cell spikes being rare and therefore highly informative. EPSP amplitude varied greatly across connected pairs (0.55–4 mV). This could reflect a distribution of electrotonic distances between synapses and recording sites. Simultaneous impalements of different dendrites in the same  $\beta$ -LN ( $n = 2$  experiments), however, show that the amplitudes of most events were the same across recording sites (Pearson's correlation  $> 0.9$ ) (Fig. 1c). Consistent with this, unitary EPSP kinetics (10–90% rise time,  $8.3$  ms  $\pm$  2.3; time to  $1 - (1/e)$  of peak,  $13.2$  ms  $\pm$  4.4) were independent of the  $\beta$ -LN recorded and, thus, of the impalement site (inset, Fig. 1b). Simultaneous dendritic recordings of different  $\beta$ -LNs ( $n = 5$  experiments), however, revealed that their synaptic backgrounds overlapped only partly (Fig. 1d; Pearson's correlation or fraction of common EPSPs, 0.1–0.3). Common EPSPs rarely had the same amplitude (Fig. 1d). Hence,  $\beta$ -LNs may each receive inputs from hundreds to thousands ( $\sim 2\%$  of 50,000 Kenyon cells) of Kenyon cells, in overlapping subsets; KC– $\beta$ -LN connections are strong on average, with target-specific strength.

Odour-evoked activity in projection neurons and Kenyon cells consists principally of sequential volleys of synchronized spikes—generally, one spike per responding neuron per oscillation cycle<sup>1,2,15</sup>.  $\beta$ -LN responses to odours also consisted typically of sequences of single phase-locked spikes, timed around the trough of several local field potential (LFP) oscillation cycles (Fig. 2a, b). The cycles when a spike was produced (usually with probability  $< 1$ ) depended on  $\beta$ -LN and stimulus identity, as illustrated in Fig. 2c, d. We conclude that, to each oscillation cycle corresponds a particular activity vector in the projection neuron<sup>2</sup>, Kenyon cell<sup>2</sup> and  $\beta$ -LN populations. By recording from pairs of  $\beta$ -LNs simultaneously during odour trials, we also observed that, when the two  $\beta$ -LNs fired one action potential during the same oscillation cycle ( $n = 4$  pairs; Fig. 2d, upper panel, asterisks), those action potentials were tightly synchronized ( $\pm 2$  ms, Fig. 2d, middle and lower panels).

A fortuitous observation provided hints of plasticity at the KC– $\beta$ -LN synapse (Fig. 3a). At trial 4 of a Kenyon cell stimulus sequence intended to explore  $\beta$ -LN integration, the  $\beta$ -LN fired a spontaneous action potential roughly at the time of the first (of 2) Kenyon-cell-evoked EPSP (Fig. 3a). At trial 5, 10 seconds after this single fortuitous pairing, the first EPSP of the pair was greatly enhanced (Fig. 3a). This suggested the possibility of spike-timing-dependent plasticity (STDP), a phenomenon thus far unknown in invertebrates but well characterized in vertebrates, in which the gain of a connection can be changed according to the temporal relationship between pre- and post-synaptic spikes<sup>8–10</sup>. We explored the consequence of pre-post temporal relationships on the KC– $\beta$ -LN synapse. A  $\beta$ -LN was impaled and stimulated alternately by two independent Kenyon cell pathways—one for pairing, one for unpaired control (Fig. 3b). Each stimulus was repeated every 10 s, with a 5-s delay between pairing and control stimuli. Pairing consisted of a single Kenyon cell (pre) stimulus and a 5-ms supra-threshold  $\beta$ -LN (post) current pulse, timed such that the delay ( $dt = t_{\text{post}} - t_{\text{pre}}$ ) between pre- and post-synaptic spikes varied between  $-60$  and  $+50$  ms. Test trials, used to measure connection strength before and after pairing, were identical to the pairing trials in all respects except in the temporal relationship between pre- and post-synaptic spike times (2.5 s apart, Fig. 3b). Two examples with controls are shown in Fig. 3c, d (for  $dt = 10$  ms and  $-4$  ms, 25 pairings each). For  $dt = 10$  ms (Fig. 3c), the paired input underwent potentiation; for  $dt = -4$  ms (Fig. 3d), it underwent depression. For both conditions, the control pathway (same  $\beta$ -LN, different Kenyon cell input) remained unchanged (Fig. 3c, d, lower panels). The changes were thus input-specific; they were

often detectable after a single pairing (see also Fig. 3a), and could be maintained for up to 25 min. We tested 26 values of  $dt$  between  $-60$  and  $+50$  ms. The resulting changes (Fig. 3e) define a classical hebbian profile<sup>8,10</sup>: the synapse is potentiated when pre- precedes post-, and depressed when post- precedes pre-, with symmetrical profiles. The changes could be fitted well with two exponential decays flanking a narrow linear range around  $t = +4$  ms ( $\tau_1 = 10.4$  ms for  $dt < -9$  ms;  $y = 3.78t - 13.1$  for  $-9$  ms  $< dt < 17.5$  ms;  $\tau_2 = 11.6$  ms for  $dt > 17.5$  ms). Several connections were tested successively with two (or more) values of  $dt$  (some positive, others negative): the same connections could undergo both depression and potentiation, depending on the value of  $dt$ . The STDP profile thus seems to be a property of each connection and not only a collective one.

We observed that the values of  $dt$  over which synaptic weights change correspond to the period of single odour-evoked oscillation cycles; hence, only within-cycle 'coincidences' may modify the connections between a Kenyon cell and its targets. The features of the STDP curve, when considered together with the timing of Kenyon cells and  $\beta$ -LNs during odour-evoked activity, have interesting

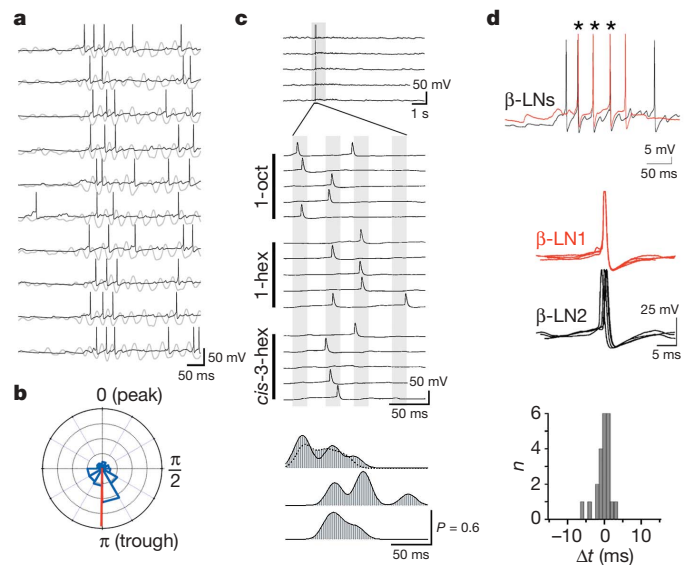


**Figure 2 |  $\beta$ -LN tuning and spike-time precision during responses to odours.** **a**, Responses of one  $\beta$ -LN to ten successive trials with odour *cis*-3-hexen-1-ol (LFP shown in grey). Note non-random timing of  $\beta$ -LN action potentials during each trial and during each oscillation cycle (calibration LFP, 250  $\mu$ V). **b**,  $\beta$ -LN action potentials lock to the trough of LFP during odour responses. Phase plot of  $\beta$ -LN action potentials during odour responses (phases plotted clockwise). Distribution (blue) constructed with data from 8  $\beta$ -LNs (average in red). **c**,  $\beta$ -LN responses are structured in time and are odour-specific (see also ref. 17). This  $\beta$ -LN responds to different odours with different discharge patterns: upper panel, response to odour 1-octanol (grey bar); middle panels, same 5 trials as in upper panel on an expanded time base, showing approximate timing of relevant oscillation cycles (grey bars) and also showing responses to 1-hexanol and *cis*-3-hexen-1-ol. Apparent spike-time jitter is due to variability of oscillation cycle duration within and across trials. In contrast, spike-time jitter across  $\beta$ -LNs, but within the same oscillation cycle of the same trial, is low (see panel **d**). Lower panel, smoothed peri-stimulus time-histogram from the trials and odours in the middle panels (in the same order). The y axis measures firing probability. Stippled line in the top peri-stimulus time-histogram shows responses to a second set of 5 trials with this odour, delivered after trials with the 2nd and 3rd odours. **d**, Spike discharges in response to odours are precisely locked across  $\beta$ -LNs. Upper panel, simultaneous recording of two  $\beta$ -LNs during odour stimulus, with spikes from both neurons in several oscillation cycles (\*). Note precise overlap. Middle panels, zoom on those action potentials, superimposed and triggered on  $\beta$ -LN1 action potential. Lower panel, distribution of spike-time jitter. Recordings as in the middle panels;  $\Delta t$  is the time difference between spikes in  $\beta$ -LNs 1 and 2, when they occur in the same oscillation cycle.

consequences. Consider the phases of Kenyon cell and  $\beta$ -LN spikes (Fig. 4a). Owing to propagation delays, Kenyon cell spikes reach their targets just before the trough of the LFP, a little before  $\beta$ -LN firing (Fig. 2a, b). Consider a cycle in which a  $\beta$ -LN spikes early ( $dt < 0$ ): some KC– $\beta$ -LN connections will undergo depression (Fig. 3e); at the next trial,  $\beta$ -LN spike time at this cycle should be delayed (Fig. 4b). If, in contrast, a  $\beta$ -LN spikes late, STDP should potentiate Kenyon cell drive to it, and thus advance spike time for that cycle (Fig. 4b). In short, the cycle-by-cycle action of STDP suggests adaptive control of  $\beta$ -LN spike phase. The need for such regulation is not unique to this system: models of cortical networks indicate that, as activity propagates through successive ‘layers’, accumulating noise can rapidly smear the temporal structure that may exist<sup>18,19</sup>. Modelling studies<sup>20–22</sup> predict that STDP, given appropriate parameters, could preserve the temporal discretization of activity through such layers.

We generated a reduced model of the KC– $\beta$ -LN circuit (Methods) and introduced the STDP rule derived from our experiments (Fig. 4c). To control the relative phases of Kenyon cells and  $\beta$ -LNs, we drew Kenyon cell spike phases from experiments<sup>2</sup>, and input weights from uniform distributions with different means: with low weights,  $\beta$ -LN spikes tended to occur late ( $dt > 0$ , Fig. 4d); with larger weights, they occurred early ( $dt < 0$ , Fig. 4d). After several trials (each with a random draw of inputs from the same distribution), STDP was allowed to modify synaptic weights for the following trials: when  $\beta$ -LN spikes occurred late ( $dt > 0$ ), Kenyon cell outputs became potentiated and  $\beta$ -LN spikes were advanced; for  $dt < 0$ , time shifts were inverted. The histograms in Fig. 4d represent spike-time distributions for 1,000 trials before (red) and after (black) STDP, for each of three conditions. These simulations were repeated 200 times (50 trials each), with 11 different Kenyon cell input distributions (Fig. 4e). Once STDP was turned on (trial 1), the evolution was

systematic and rapid, leading to the adaptive up- or downregulation of input weights, firing phase and response intensity (top, middle and bottom, respectively, all averages; Fig. 4e). Given that the model is entirely constrained by experiments, it is noteworthy that the mean phase of the first  $\beta$ -LN spike at steady state ( $\pi$  rad, Fig. 4e), matches precisely that measured experimentally (Fig. 2b).

To test directly the effect of STDP on  $\beta$ -LN output, we next manipulated  $\beta$ -LN spike timing during responses to odours *in vivo*: if our model is correct, such manipulations should change the output of the odour-activated Kenyon cells onto that  $\beta$ -LN and, thus, generate predictable shifts in its spike phase. During odour stimuli, short current pulses locked to selected cycles of the LFP were injected in a  $\beta$ -LN: a negative pulse (b, Fig. 4f) was injected during the cycles and phase when the  $\beta$ -LN would naturally fire (to prevent stimulus-evoked spikes), and a positive pulse (c, Fig. 4f) was injected at a desired phase, for those same cycles (that is, at an abnormal time relative to the Kenyon cell inputs that would normally drive the recorded  $\beta$ -LN). An example is shown for four consecutive cycles in Fig. 4g. After several such pairing trials, current injection was terminated and  $\beta$ -LN-firing phase over the next trials was compared to that before pairing. Figure 4h plots the effects of one such manipulation ( $dt > 0$ ): as predicted, an artificial phase-delay caused a corrective phase-advance. Twenty distinct experiments were carried out in six  $\beta$ -LNs; the expected phase shifts were observed in 16 of those 20 (Mann–Whitney:  $P < 0.001$ ) (Fig. 4i). This is consistent with an adaptive role for STDP in the fine-tuning of  $\beta$ -LN spike-phase, and may explain the tight synchronization of  $\beta$ -LNs (Fig. 2d). Hence, STDP helps preserve the discrete and periodic structure of olfactory representations as they flow through the mushroom bodies.

We showed that the connections made by Kenyon cells to  $\beta$ -LNs are excitatory, strong on average, variable across pairs, and plastic. Plasticity follows time-sensitive hebbian associativity rules<sup>8–10</sup> and

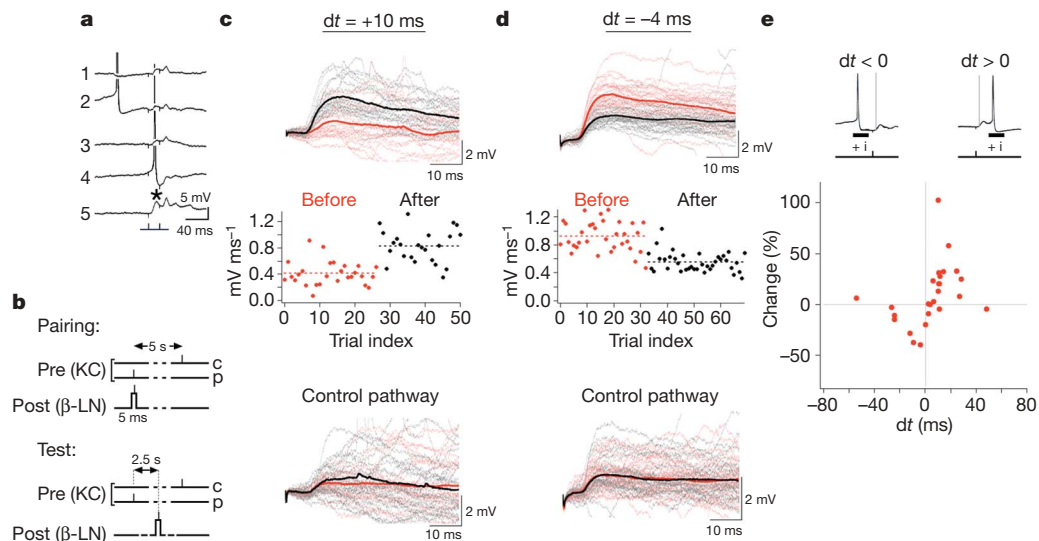


**Figure 3 | Hebbian spike-time-dependent plasticity at the KC– $\beta$ -LN synapse.** **a**, Effect of single, near-coincident spikes in pre- and post-synaptic neurons on the Kenyon cell to  $\beta$ -LN synapse. The  $\beta$ -LN is held from a dendrite at normal resting potential *in vivo*, and subjected to paired Kenyon cell stimuli at 20-ms intervals (first and second stimuli in train are from different Kenyon cell electrodes). At trial 4, the effect of the first stimulus sums with an on-going slow depolarization, causing a  $\beta$ -LN action potential. At trial 5, the first EPSP (asterisk) is dramatically enhanced. **b**, Stimulation protocols to probe STDP. For ‘pairing’, the  $\beta$ -LN is depolarized with a 5-ms DC pulse, causing a single  $\beta$ -LN spike in a window around the time of the Kenyon cell pairing stimulus (p). We tested the effects of 5 to 25 successive pairings (10-s intervals); all evoked STDP. Control Kenyon cell stimulus (c) is offset by 5 s relative to the  $\beta$ -LN current pulse. ‘Test’, same protocol as pairing, except that Kenyon cell and  $\beta$ -LN stimuli are 2.5 s apart.

**c**, Potentiation of KC– $\beta$ -LN connection after 25 pairings with  $dt = 10$  ms. Upper panel, superimposed before- and after-trials, with their averages (bold lines). Middle panel, EPSP slope against trial index, with 25 pairings between the before- and after- periods. Stippled lines are average slopes over corresponding trials. Lower panel, a control, recorded at the same time with a second Kenyon cell pathway, offset by 5 s with respect to the  $\beta$ -LN spike, and showing no significant change. **d**, Depression of KC– $\beta$ -LN connection after 25 pairings with  $dt = -4$  ms. Panels as in panel **c**. **e**, STDP plot for 26 values of  $dt = t_{\text{post}} - t_{\text{pre}}$ , where  $dt$  is measured as the delay between the  $\beta$ -LN spike ( $t_{\text{post}}$ , caused by intracellular current injection, + i) and the  $\beta$ -LN EPSP onset ( $t_{\text{pre}}$ , grey line, upper panels). EPSP onset time is used (rather than Kenyon cell stimulus time) because Kenyon cell spike time at the  $\beta$ -LN synapse is delayed from stimulus time, owing to spike propagation (see Fig. 4a). Note the zero-crossing is slightly offset from  $dt = 0$  (lower panel).

is constrained to within-cycle interactions between pre- and post-synaptic neurons. STDP is therefore not specific to vertebrates or cortical architectures. We do not know the molecular underpinnings of STDP in this system, or whether STDP might confer the associative features usually ascribed to mushroom bodies<sup>4–7</sup>. The fly and honeybee genomes both reveal coding sequences for *N*-methyl-D-aspartate (NMDA) receptor subunits<sup>13,23</sup> and some *Drosophila* behavioural results<sup>24</sup> are compatible with STDP learning rules<sup>25</sup>. One hypothesis, readily testable here, is that STDP provides associativity by tagging transiently the subset of synapses activated simultaneously by the odour, before the conditional arrival of a slower, non-specific reward signal<sup>26</sup>.

Our results reinforce the proposed importance of spike timing for this, and possibly other, olfactory system(s)<sup>1,2</sup>: Kenyon cells act as coincidence detectors for synchronized projection neuron input<sup>2</sup>,  $\beta$ -LNs act as coincidence detectors for Kenyon cell input; because STDP helps enhance  $\beta$ -LN synchronization, we infer that spike

timing must be relevant also for the processing of  $\beta$ -LN output. These results indicate that the oscillation cycle—a temporal unit of processing first defined by negative feedback in the antennal lobe<sup>14</sup>—is actively preserved in at least three successive layers of processing (projection neurons, Kenyon cells and  $\beta$ -LNs). It will be interesting to assess whether all Kenyon cell outputs obey the same STDP rules, and if these rules are themselves subject to learning-related modifications. Indeed, Kenyon cells seem to communicate with one another through axo-axonal chemical synapses<sup>27</sup>. Given the dynamics of projection neuron/Kenyon cell activity vectors in response to odours<sup>1,2,15</sup>, the possibility that Kenyon cell–Kenyon cell synapses also undergo STDP suggests a mechanism for sequence learning<sup>28</sup>, similar to principles proposed for spatial map formation in rodents<sup>29,30</sup>; here, however, the learned sequences have no relation to movement in physical space. The existence of such similarities (synaptic learning rules, and synchronized and sequential neural activity patterns) may bring us closer to understanding the

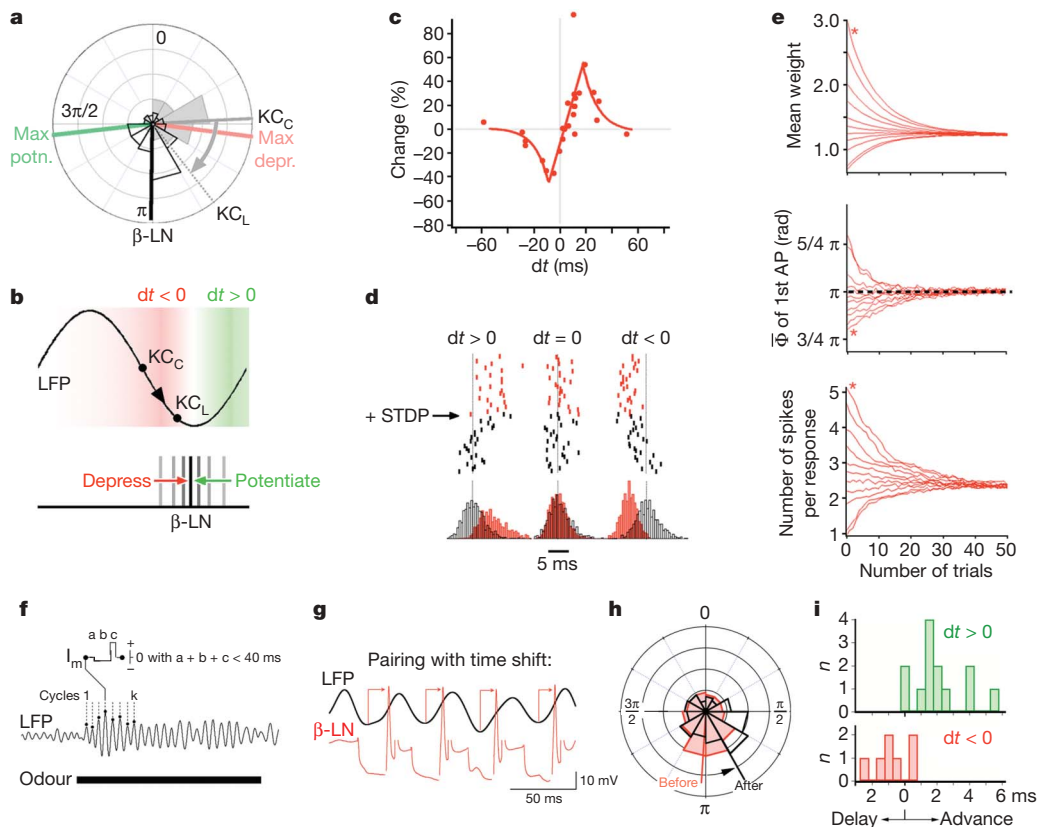


**Figure 4 | The effect of STDP on  $\beta$ -LN spike timing.** **a**, Polar plot of Kenyon cell spike phase in the calyx (somata) ( $KC_C$ ) and in the  $\beta$ -lobe ( $KC_L$ ), and  $\beta$ -LN spike phase (from dendrites in the  $\beta$ -lobe) relative to the LFP (in the calyx). All measurements from experiments. Green and red lines indicate extrema of the STDP curve (see panel **c**). **b**, Schematic of temporal relationships between LFP, Kenyon cell spike time,  $\beta$ -LN spike time and the STDP rule. The Kenyon cell mean spike time in the calyx ( $KC_C$ ) is about  $\pi/2$  after the LFP peak, and near the LFP trough in the  $\beta$ -lobe ( $KC_L$ ), owing to propagation delay.  $\beta$ -LN mean spike time in the  $\beta$ -lobe is at the LFP trough ( $\pi$  rad). The STDP curve is represented in colour gradients. The predicted effect of STDP on  $\beta$ -LN spike time is schematized underneath. If the  $\beta$ -LN spike occurs early, STDP should depress late Kenyon cell inputs (in this oscillation cycle), delaying this  $\beta$ -LN spike at the next opportunity. The converse applies if the  $\beta$ -LN spike occurs late. **c**, The STDP fit (two exponentials flanking a linear segment, see text) overlaid on experimental data. **d**, Simulations of STDP on  $\beta$ -LN spike time (rasters) (model  $\beta$ -LN excited by 10 model Kenyon cells during one LFP cycle). First trial at top. Three conditions are illustrated: left panel, low input weights (mean, 1.8 mV; range, 3 mV), causing late  $\beta$ -LN-spike times ( $dt > 0$ ); when STDP is turned on, potentiation shifts  $\beta$ -LN spikes to earlier times. Right panel, high input

weights (mean, 9 mV; range, 3 mV); when STDP is turned on, depression delays  $\beta$ -LN-spike times. Middle panel, intermediate weights, causing no change. Histograms show the distribution of  $\beta$ -LN spike times before (red) and after (black) STDP (1,000 runs per condition). **e**, Evolution of  $KC$ – $\beta$ -LN weights (upper panel),  $\beta$ -LN mean spike phase (middle panel) and number of spikes per response (lower panel) over 50 trials following onset of STDP (at trial 1). AP, action potential. Each curve is an average of 200 simulations (11 different input distribution means). Asterisks indicate a corresponding condition in the three plots. **f**, Schematic of experimental design. LFP cycles (1...*k*) during which the recorded  $\beta$ -LN-produced action potentials are selected. Peaks of LFP are used to trigger a sequence of current ( $I_m$ ) pulses (a, b, c) into the  $\beta$ -LN (one such sequence per oscillation cycle). The a-b-c sequence lasts less than one oscillation cycle, and is repeated for all selected cycles, over several trials. **g**, Example of protocol described in panel **f**, such that the  $\beta$ -LN spike is phase-delayed to  $\sim 3/2\pi$  (arrows). (Interrupted segments of  $\beta$ -LN potential trace are bridge-balance artefacts.) **h**, Phase plot of spikes in one  $\beta$ -LN before and after pairing (10 trials each), as in panel **g**. Fifteen pairing trials (estimated  $dt = 17$  ms). **i**, Distributions of pairing-induced mean phase shifts, measured in 20 separate experiments (6  $\beta$ -LNs; mean  $\pm$  s.e.m. =  $-0.74 \pm 0.4$  ms versus  $2.0 \pm 0.4$  ms).

relationships between circuit dynamics, architecture and learning in the brain.

## METHODS SUMMARY

All results were obtained *in vivo* from locusts (*Schistocerca americana*) in an established, crowded colony. Odours were delivered by injection within a constant stream of dessicated air. The results presented here originate from recordings of over 50  $\beta$ -LNs in 40 locusts. Kenyon cells were stimulated electrically from their soma, using gold-electroplated tetrodes or intracellular electrodes.  $\beta$ -lobe neurons were recorded from their dendrites in the  $\beta$ -lobe with glass micropipettes. Field potential recordings were carried out from the Kenyon cell soma cluster, using twisted-wire tetrodes. Stimulation protocols and data analysis were carried out using specialized software (LabView, National Instruments; Igor, Wavemetrics).

**Full Methods** and any associated references are available in the online version of the paper at [www.nature.com/nature](http://www.nature.com/nature).

**Received 26 April; accepted 1 June 2007.**

**Published online 20 June 2007.**

- Mazor, O. & Laurent, G. Transient dynamics versus fixed points in odor representations by locust antennal lobe projection neurons. *Neuron* **48**, 661–673 (2005).
- Perez-Orive, J. *et al.* Oscillations and sparsening of odor representations in the mushroom body. *Science* **297**, 359–365 (2002).
- Wilson, R. I., Turner, G. C. & Laurent, G. Transformation of olfactory representations in the *Drosophila* antennal lobe. *Science* **303**, 366–370 (2004).
- deBelle, J. S. & Heisenberg, M. Associative odor learning in *Drosophila* abolished by chemical ablation of mushroom bodies. *Science* **263**, 692–695 (1994).
- Dubnau, J., Grady, L., Kitamoto, T. & Tully, T. Disruption of neurotransmission in *Drosophila* mushroom body blocks retrieval but not acquisition of memory. *Nature* **411**, 476–480 (2001).
- Yu, D., Keene, A. C., Srivatsan, A., Waddell, S. & Davis, R. L. *Drosophila* DPM neurons form a delayed and branch-specific memory trace after olfactory classical conditioning. *Cell* **123**, 945–957 (2005).
- Zars, T., Fischer, M., Schulz, R. & Heisenberg, M. Localization of a short-term memory in *Drosophila*. *Science* **288**, 672–675 (2000).
- Bi, G. Q. & Poo, M.-M. Synaptic modifications in cultured hippocampal neurons: dependence on spike timing, synaptic strength, and postsynaptic cell type. *J. Neurosci.* **18**, 10464–10472 (1998).
- Markram, H., Lubke, J., Frotscher, M. & Sakmann, B. Regulation of synaptic efficacy by coincidence of postsynaptic APs and EPSPs. *Science* **275**, 213–215 (1997).
- Roberts, P. D. & Bell, C. C. Spike timing dependent synaptic plasticity in biological systems. *Biol. Cybern.* **87**, 392–403 (2002).
- Clyne, P. J. *et al.* A novel family of divergent seven-transmembrane proteins: candidate odorant receptors in *Drosophila*. *Neuron* **22**, 327–338 (1999).
- Vosshall, L. B., Wong, A. M. & Axel, R. An olfactory sensory map in the fly brain. *Cell* **102**, 147–159 (2000).
- The Honeybee Genome Sequencing Consortium. Insights into social insects from the genome of the honeybee *Apis mellifera*. *Nature* **443**, 931–949 (2006).
- MacLeod, K. & Laurent, G. Distinct mechanisms for synchronization and temporal patterning of odor-encoding neural assemblies. *Science* **274**, 976–979 (1996).
- Wehr, M. & Laurent, G. Odour encoding by temporal sequences of firing in oscillating neural assemblies. *Nature* **384**, 162–166 (1996).
- Jortner, R., Farivar, S. S. & Laurent, G. A simple connectivity scheme for sparse coding in an olfactory system. *J. Neurosci.* **27**, 1659–1669 (2007).
- MacLeod, K., Backer, A. & Laurent, G. Who reads temporal information contained across synchronized and oscillatory spike trains? *Nature* **395**, 693–698 (1998).
- Diesmann, M., Gewaltig, M. O. & Aertsen, A. Stable propagation of synchronous spiking in cortical neural networks. *Nature* **402**, 529–533 (1999).
- Vogels, T. P., Rajan, K. & Abbott, L. F. Neural network dynamics. *Annu. Rev. Neurosci.* **28**, 357–376 (2005).
- Arthur, J. V. & Boahen, K. *Advances in Neural Information Processing*. (eds Sholkopf, B. & Weiss, Y.) 75–82 (MIT Press, 2006).
- Suri, R. E. & Sejnowski, T. J. Spike propagation synchronized by temporally asymmetric Hebbian learning. *Biol. Cybern.* **87**, 440–445 (2002).
- Zhigulin, V. P., Rabinovich, M. I., Huerta, R. & Abarbanel, H. D. Robustness and enhancement of neural synchronization by activity-dependent coupling. *Phys. Rev. E* **67**, 021901 (2003).
- Ultsch, A., Schuster, C. M., Laube, B., Betz, H. & Schmitt, B. Glutamate receptors of *Drosophila melanogaster*. Primary structure of a putative NMDA receptor protein expressed in the head of the adult fly. *FEBS Lett.* **324**, 171–177 (1993).
- Tanimoto, H., Heisenberg, M. & Gerber, B. Experimental psychology: event timing turns punishment to reward. *Nature* **430**, 983 (2004).
- Drew, P. J. & Abbott, L. F. Extending the effects of spike-timing-dependent plasticity to behavioral timescales. *Proc. Natl Acad. Sci. USA* **103**, 8876–8881 (2006).
- Frey, U. & Morris, R. G. Synaptic tagging: implications for late maintenance of hippocampal long-term potentiation. *Trends Neurosci.* **21**, 181–188 (1998).
- Leitch, B. & Laurent, G. GABAergic synapses in the antennal lobe and mushroom body of the locust olfactory system. *J. Comp. Neurol.* **372**, 487–514 (1996).
- Nowotny, T., Rabinovich, M. I., Huerta, R. & Abarbanel, H. D. Decoding temporal information through slow lateral excitation in the olfactory system of insects. *J. Comput. Neurosci.* **15**, 271–281 (2003).
- Blum, K. I. & Abbott, L. F. A model of spatial map formation in the hippocampus of the rat. *Neural Comput.* **8**, 85–93 (1996).
- Mehta, M. R., Lee, A. K. & Wilson, M. A. Role of experience and oscillations in transforming a rate code into a temporal code. *Nature* **417**, 741–746 (2002).

**Supplementary Information** is linked to the online version of the paper at [www.nature.com/nature](http://www.nature.com/nature).

**Acknowledgements** This work was supported by an NIH training grant, grants from the NIDCD, and the Lawrence Hanson Fund. We thank E. Schuman, I. Fiete, M. Murthy, M. Papadopoulou, O. Mazor, V. Jayaraman and the reviewers for their helpful comments.

**Author Information** Reprints and permissions information is available at [www.nature.com/reprints](http://www.nature.com/reprints). The authors declare no competing financial interests. Correspondence and requests for materials should be addressed to G.L. ([laurentg@caltech.edu](mailto:laurentg@caltech.edu)).

## METHODS

**Preparation and stimuli.** All results were obtained *in vivo* from locusts (*Schistocerca americana*) in an established, crowded colony. Young adults of either sex were immobilized, with two antennae intact for olfactory stimulation. The brain was exposed and de-sheathed as previously described<sup>2</sup>. Odours were delivered by injection of a controlled volume of odourized air within a constant stream of dessicated air. Teflon tubing was used at and downstream from the mixing point to prevent odour lingering and cross-contamination. Odours were used at 10% vapour pressure further diluted in the dessicated air stream. The results presented here originate from recordings of over 50  $\beta$ -LNs in 40 locusts.

**Electrical stimulation.** Twisted-wire tetrodes obtained from FHC (number CE4B75) were modified for monopolar stimulation, with the casing serving as the anode. The tips of the tetrodes were splayed such that the distance between the exposed tips was approximately equal to 60% of the diameter of the mushroom body calyx. The exposed end of the stimulating electrode was embedded among Kenyon cell somata. The tetrodes were electroplated with gold solution to reduce the impedance to between 200 and 350 k $\Omega$  at 1 kHz. Stimulating currents (5–50  $\mu$ A, 0.1 ms) were generated by an STG1000 Multichannel System. The number of consecutive pairing trials varied between 5 and 25, at 10-s intervals. Propagation delays for the Kenyon cell action potentials were measured as the delay between a Kenyon cell soma stimulus and the extracellular spike volley recorded in the  $\beta$ -lobe, at the level of the  $\beta$ -LN dendritic recordings<sup>31</sup>.

**Intracellular recordings.** Sharp electrode recordings from the dendrites of  $\beta$ -lobe neurons were made with borosilicate glass micropipettes (DC resistance, 100 M $\Omega$ ) filled with 3 M K acetate. Input resistance was around 300 M $\Omega$ . The cell type from which the data are derived could be recognized by several characteristics, including response to odour, sub-threshold baseline activity profile, and response to electrical stimulation of Kenyon cells. A series of pilot experiments, in which the cells were stained intracellularly by injection of 6% cobalt hexamine, confirmed that cells with these physiological characteristics belong to a specific morphological class (see Supplementary Fig. 1). EPSP slopes were measured from linear fits to voltage trace between 10% and 90% of rising phase. Recordings from  $\beta$ -LNs were always made from dendrites in the  $\beta$ -lobe (the largest dendrites are often several  $\mu$ m in diameter). That these recordings were not from Kenyon cell axons is guaranteed by the fact that Kenyon cell axons are too small for intracellular impalement (100–400 nm diameter<sup>27</sup>). This identity of  $\beta$ -LNs was confirmed by dye injection. Kenyon cell intracellular recordings were always made from their somata (5–7  $\mu$ m diameter).

**Field recordings.** Twisted-wire tetrodes obtained from FHC (number CE4B75) were used for extracellular recordings of the local field potential (LFP). For these recordings, the tip was cut with fine scissors and each channel tip was electroplated with gold solution to reduce the impedance to between 200 and 350 k $\Omega$  at 1 kHz. These recordings were made with a custom-built 16-channel pre-amplifier and amplifier. Two to four tetrodes were used simultaneously. The pre-amp has a unitary gain, and the amplifier gain was set to 10,000 $\times$ . For pairing experiments during odour stimuli (Fig. 4f–i), the LFP was low-pass filtered on line and fed through a real-time peak-detection algorithm. Each detected peak was given a rank order (1...k) and the cycles during which the recorded  $\beta$ -LN produced an action potential were identified. Because of inter-trial variability of LFP and small uncertainty about cycle ranking in each trial, we typically selected eight consecutive oscillation cycles centred on the cycles of interest. During each one of those 8 consecutive cycles, a current-pulse sequence (a–c, Fig. 4f) was injected into the  $\beta$ -LN dendrite so as to phase-advance ( $b > 0$ ;  $c < 0$ ) or phase-delay ( $b < 0$ ;  $c > 0$ ) its odour-evoked spikes. This pulse sequence was started again at each LFP peak of the selected cycles.

**Simulations.** A leaky integrate-and-fire model ( $R = 300$  M $\Omega$ ,  $\tau = 20$  ms) was implemented in Igor (Wavemetrics, Lake Oswego, Oregon). Spiking threshold and after-hyperpolarization were estimated from intracellular recordings. A single oscillation cycle was modelled as 10 inputs convolved with a current waveform derived from dual KC– $\beta$ -LN recordings. The number of inputs per cycle was based on KC– $\beta$ -LN connectivity estimates from dual intracellular recordings and from  $\beta$ -LN baseline sub-threshold activity, as well as on the average Kenyon cell population response time course<sup>1–3</sup> and response probability<sup>2</sup>. The specific Kenyon cell spike times were drawn randomly at every trial from the Kenyon cell spike time distribution. The weights at the start of each simulation were drawn randomly from a distribution similar to that observed experimentally, and scaled for different simulations to evaluate the effect on the spiking response in the presence and absence of STDP. The STDP rule was modelled, as described in the text, by two exponentials flanking a linear region (fitted to data by minimizing Chi-square; Igor curve-fitting). When STDP was invoked, every trial was followed by an update of the weights, on the basis of  $dt$ , as dictated by the fitted STDP curve (Fig. 4).

31. Perez-Orive, J., Bazhenov, M., Stopfer, M. & Laurent, G. Intrinsic and circuit properties favor coincidence detection for decoding oscillatory input. *J. Neurosci.* **24**, 6037–6047 (2004).